PAPER

Check for updates

Mechanoluminescent-energy harvesting bimodal sensors for self-powered communication sensors

Sugato Hajra, [ID] [a] Swati Panda,[a] Kushal Ruthvik Kaja,[a] Seongkyu Song, [ID] [b] Yeonkyeong Ryu,[c] Basanta Kumar Panigrahi,[d] Naratip Vittayakorn,[e] Ju-Hyuck Lee, [ID] *[c] Soon Moon Jeong [ID] *[fg] and Hoe Joon Kim [ID] *[a]

Mechanoluminescence (ML) is the emission of light triggered by mechanical stress. In the meantime, accurate, quantitative force measurement is made possible by piezoelectricity, which transforms mechanical deformation into electrical signals. A deep insight into the mechanical interactions, such as strain-based phenomena, is achieved by integrating ML and piezoelectricity into a single device. In this study, a composite based on ZnS:Cu–polydimethylsiloxane (PDMS) is developed to achieve this dual functionality for ML-based optical responses and piezoelectric-based electrical output. The presence of piezoelectricity in PDMS–ZnS:Cu composites was traced using piezo force microscopy (PFM) imaging. Various mechanical stimuli of pressing, stretching, and bending are applied to evaluate the performance of the device. Under a force of 5 N, the piezoelectric nanogenerator (PENG) device generates a voltage of 17 V and a current of 70 nA. Additionally, ML and PENG effects are employed for underwater communications. A signal processing technique is further utilized for the classification of voltage signals produced during underwater communications. This self-powered dual-mode sensor has great potential for use in energy harvesting, wearable technology, and battery-free systems, opening the door to more intelligent and responsive user interfaces.

1. Introduction

Mechanoluminescence (ML) provides a fast and clear method to detect a type of light emission induced by physical deformation.[1] This characteristic makes ML highly beneficial across numerous domains, including medical diagnostics, motion analysis, smart textiles, surveillance technologies, energy generation, energy-efficient screens, and force detection.[2–7] While ML delivers an instantaneous optical reaction to mechanical forces, accurately linking these signals with applied stress or movement remains difficult. Variables such as surrounding illumination levels, detector choice, and standardization methods can greatly impact measurement precision. To overcome these obstacles, recent progress in ML studies has concentrated on merging ML with additional detection mechanisms to improve both numerical reliability and application adaptability.

With the increasing amount of demand in the consumer electronics market, the need for alternative renewable energy sources has become critical.[8,9] The battery is a common power source in recent days, which faces numerous challenges such as low life, limited charging facilities, limited accessibility, and waste after use.[10] Among these, mechanical energy from sources such as wind and vibrations has gained significant attention due to its widespread availability.[11–15] In 2006, Wang *et al.* pioneered the use of piezoelectric nanogenerators (PENGs) based on zinc oxide (ZnO) nanowires for converting mechanical energy into electricity, demonstrating their potential for powering nanosystems.[16] Over time, various piezoelectric materials, including semiconductors, polymers, and ceramics, have been explored to improve energy conversion efficiency.[17–21] PENG was further utilized in various applications such as sensing, biomedical devices, acoustic applications, and energy harvesting.[22–25]

The intensity of ML light and sensor calibration make it challenging for practical applications, limited by factors that affect measurement accuracy. Hence, energy harvesting with

*[a] Department of Robotics and Mechatronics Engineering, Daegu Gyeongbuk Institute of Science and Technology, Daegu, 42988, Republic of Korea.
E-mail: joonkim@dgist.ac.kr*

[b] Division of Energy and Environmental Technology, DGIST, Daegu, 42988, Republic of Korea

*[c] Department of Energy Science & Engineering, Daegu Gyeongbuk Institute of Science & Technology (DGIST), Daegu, Republic of Korea.
E-mail: jhlee85@dgist.ac.kr*

[d] Department of Electrical Engineering, Siksha O Anusandhan University, Bhubaneswar-751030, India

[e] Department of Chemistry, School of Science, King Mongkut's Institute of Technology, Ladkrabang, Bangkok 10520, Thailand

*[f] Department of Advanced Technology, DGIST, Daegu, 42988, Republic of Korea.
E-mail: smjeong@dgist.ac.kr*

[g] Department of Interdisciplinary Engineering, DGIST, Daegu, 42988, Republic of Korea

This journal is © The Royal Society of Chemistry 2025

J. Mater. Chem. C, 2025, **13**, 19297–19307 | **19297**

PENG and triboelectric nanogenerator (TENG) can improve ML-based sensing without the need for external power sources and enable self-powered operations.[26] These nanogenerators can help with quantitative force assessment by converting mechanical impulses into electrical signals, along with optical output generated by ML. This integration advances wearables, security, and healthcare applications by increasing accuracy, dependability, and adaptability.

Sohn et al. created a device that combines ML with piezo-resistive sensing, allowing the generation of optical and electrical signals simultaneously.[27] This method is particularly useful because it ensures accurate electrical output detection along with ML generation. Wang et al. created an ML-based sensor array with a single-electrode TENG, which could replace piezoresistive sensors requiring an extra power source.[28] For both triboelectric energy harvesting and ML-based intensity detection, they utilized the PDMS–ZnS:Mn composites-based device platform. Zhang et al. created an electronic skin based on triboelectric-mechanoluminescence that recognizes finger movements by gathering triboelectric energy.[29] This idea was further developed by He et al. using a strain sensor platform that operated in dual-mode TENG and ML for human motion monitoring.[30] Further, Hajra et al. synthesized polymer composite-based PDMS–ZnS:Cu for simultaneous energy harvesting and ML emission, which paves the way for emerging safety applications and observing wind speed.[26,31] ZnS:Cu phosphor offers strong ML with high brightness, excellent durability, and rapid response under mechanical stimuli.[32] Additionally, it exhibits stable piezoelectric properties, making it ideal for energy harvesting applications.

Doped ZnS phosphors offer significant benefits for mechanoluminescent applications.[33] Incorporating elements like copper or manganese into the ZnS lattice enables consistent light emission under mechanical stress without the need for pre-activation.[34] ZnS:Cu, in particular, can emit light reliably over 100 000 cycles, making it highly suitable for real-world use.[35] While the exact mechanism behind its self-recovery luminescence remains under investigation, interest in its functional applications continues to grow. For choosing the polymer matrix certain consideration must be taken into account such as: (1) high transparency of the polymer is essential to allow efficient emission of ML light; (2) sufficient elasticity is needed to endure mechanical deformation and preserve the flexibility of the ML system; (3) strong negative triboelectric properties are crucial for enhancing ML brightness by promoting effective interfacial charge accumulation, especially under variable environmental conditions.[36–39]

Jeong et al. provided a strategic framework for selecting optimal polymer matrices such as epoxy resin, polyurethane, polydimethylsiloxane, dragon skin, and ecoflex to achieve both high stretchability and luminescent efficiency.[40] It reveals the critical role of polymer–phosphor interactions and triboelectric effects in enhancing mechanoluminescence under extreme elasticity. Huang et al. highlighted zinc sulfide-based mechanoluminescent materials as durable, flexible, and self-powered light sources for next-generation optoelectronics.[33] It offers foundational insights into ML mechanisms and design strategies for

advanced applications such as sensing, imaging, and energy conversion. Wang et al. presented a low-cost, high-performance ML hybrid from waste eggshells.[41] Using waste eggshells allows for a simple, low-cost synthesis of ML hybrids while enhancing their uniform color emission (red, green, or blue), brightness, and overall durability, advancing sustainable design for real-world mechanoluminescent applications. Sun et al. showed a stretchable, self-powered ML photonic skin enabling real-time underwater communication and monitoring.[42] Its auxetic design offers superior adaptability, durability, and signal clarity for harsh marine environments.

Many existing ML-integrated hybrid platforms incorporate triboelectric-based sensors as a key element. However, the PENG-based device is not explored in comparison to TENG during the design of a hybrid ML integrated platform. Notably, the PENG offers decreased susceptibility to material fatigue and physical wear due to its encapsulation layer. PENGs reliably convert mechanical energy into electricity regardless of location or lighting. They efficiently harvest sustainable biomechanical energy, making them ideal for portable, wearable, and eco-friendly power solutions. In light of these benefits, the main focus of our research is on integrating ML with a PENG energy harvester to develop a dual-mode platform that can produce both electrical response and light emission in reaction to external mechanical impact.

The majority of the previous studies showcase the use of lead-based ceramics with high piezoelectric coefficients to be utilized in PENG.[43–45] Many industries are slowly replacing the lead-based ceramics to develop the next generation of electronics, owing to the toxicity aroused from lead can lead to health hazards with long exposures.[46] Hence, an alternative solution needs to be introduced to overcome this challenge, which is lead-free ceramics. Some works based on $BaTiO_3$, $SrTiO_3$, $CaTiO_3$, biomaterials, and polymer composites are synthesized and used for multiple device applications based on PENG.[17,47–50] They are safe for humans and possess excellent biocompatibility. Their output conversion is still lower than that of lead-based devices. Despite this, lead-free-based ceramics or polymers open up ample opportunities for combining piezoelectric materials with ML devices in a single platform.

The present study focuses on incorporating a lead-free piezoelectric material, ZnS:Cu, into polydimethylsiloxane (PDMS) to make a composite and develop a single platform to capture the energy and light emission. The piezoelectric sensor must effectively harvest energy from various mechanical stimuli such as bending, stretching, and pressing. The ideal ZnS:Cu concentration in PDMS was utilized for maximal voltage output, and ML intensity was observed. The piezoelectric coefficient was studied for piezoelectric composite PDMS–ZnS:Cu using piezo force microscopy. The ML + PENG hybrid device was attached to the wrist, and by a bending motion, various underwater signaling was performed, opening the ability of these technologies for smart wearable interfaces, advanced surveillance systems, and sustainable power generation. Further, this type of signaling can be utilized for hazard detection and communication systems by interpreting electrical outputs and luminescent responses

19298 | J. Mater. Chem. C, 2025, **13**, 19297–19307

This journal is © The Royal Society of Chemistry 2025

through sophisticated signal processing techniques for instant decision-making. Hence, the importance of this work can be highlighted as PDMS–ZnS:Cu composite that combines piezo-electricity and mechanoluminescence, enabling simultaneous optical and electrical responses to mechanical stimuli, as shown in this work. The intrinsic bimodal functionality enables real-time, self-powered sensing even underwater.

2. Experimental techniques

The ZnS:Cu microparticles, serving as the primary phosphor for the ML platform, were sourced from Global Tungsten & Powders Corp. These microparticles had an average size ranging between 20 and 30 μm. These particles were blended with PDMS (ELASTOSIL RT601, Wacker) to form the composites. To prepare the composites, PDMS was blended in a 9:1 (monomer:hardener) ratio. Following this, ZnS:Cu was incorporated into the PDMS mixture at a 7:3 weight ratio, which was optimized to maximize brightness while preserving material softness. Additionally, a large amount of introduction of fillers in the PDMS may lead to material fracture, ultimately lowering the PENG output and intensity of illumination. The curing of the PDMS–ZnS:Cu composite was carried out inside an oven at 70 °C for 30 min. Fig. S1 shows the sheet resistance measurement of AgNWs, and PDMS–ZnS:Cu embedded AgNWs, as well as the resistivity measurement equipment using the four-point probe method (M/S DASOL ENG FPP-40K).

The morphology of PDMS–ZnS:Cu composites was characterized utilizing a field-emission scanning electron microscope (FE-SEM) (SU-8230, Hitachi, Japan). An XE7 microscope (Park Systems) was used to obtain PFM images, which included topography, amplitude, and phase, using a Pt-coated NSC36 B cantilever with a spring constant of about 2 N-m, while the 1 × 1 μm scan size was chosen during the scanning. At SLRI, Thailand, synchrotron radiation X-ray tomographic microscopy (XTM) was carried out at beamline BL1.2 W. A 2.2-T multipole wiggler running at 150 mA and 1.2 GV within the Siam Photon Source produced the X-ray synchrotron source. Filtered poly-chromatic X-ray beams with a mean energy of 12.5 kV were used in the experiment, and for all imaging operations, the source and the sample were kept 34 meters apart. Following data collection, X-ray projections were standardized using a flat-field correction. Octopus software was used to reconstruct tomographic datasets, and Drishti software made segmentation analysis and sample volume display in three dimensions easier.

To trace the electrical performance, a linear motor (LINmot, USA) was used to apply periodic pressure, while an electrometer (6514, Keithley, USA) recorded the output of the device. To record the ML spectra, a spectrometer (QEPro., Ocean Optics) was employed. The stretching tester was utilized to stretch and bend the composites. The ML pictures were captured by a phone camera (M-S Samsung, South Korea). To test ML signals, mechanical stimuli (e.g., stretching or bending force) are applied using a homemade stretching-relaxing apparatus subject to a constant, and light emission is captured using a

spectrometer in a dark environment. For piezoelectric signal measurements, electrodes are connected to the sample, and voltage or current is recorded using an electrometer (M/S Keithley 6514, USA) during periodic force applied by the linear motor.

3. Results and discussion

The pure PDMS and PDMS–ZnS:Cu samples exhibit different properties according to the PFM investigation, as shown in Fig. 1a and b. With height variations of ± 10 nm, the pure PDMS displays a chevron-like topographical pattern. However, it also displays a noisy phase pattern and negligible piezoelectric response in its amplitude, suggesting random domain orientations. The PDMS–ZnS:Cu, on the other hand, exhibits improved piezoelectric characteristics, as seen by its modified topographical pattern, stronger amplitude response between 0 and 1.1 V, and a more uniform phase distribution that suggests improved domain alignment. Flexible piezoelectric polymers often exhibit a moderate but dependable piezoelectric response, as evidenced by the observed effective piezoelectric coefficient (d_{33}) of 5.1 pm V^{-1} with a standard error of 0.87. An alternating current (AC) voltage ranging from 1 to 5 V was applied between the sample and probe tip to generate an electric field, thereby activating the reverse piezoelectric effect.

The resulting mechanical displacement and polarity variations in response to the applied voltage were examined to determine the effective piezoelectric coefficient (d_{33}). To ensure accuracy, the d_{33} value was calibrated using X-cut quartz, which has a well-established piezoelectric coefficient of 2.3 pm V^{-1}. The findings revealed that pure PDMS exhibited no measurable piezoelectric response, whereas the PDMS–ZnS:Cu composite displayed an effective d_{33} of 5.1 pm V^{-1}, confirming its piezo-electric nature. A DC bias voltage sweep from -10 to 10 V across the PDMS–ZnS:Cu composite reveals a characteristic butterfly-shaped strain–voltage curve (Fig. S2a), indicative of nanodeflection of the inherent dipoles under mechanical input. This behavior reflects the presence of the reverse piezoelectric effect within the composite.[51] Additionally, the polarization–voltage curve (Fig. S2b) exhibits a near 180° phase shift, representing the typical switching of the ferroelectric domains of the functional layer.[52] These observations collectively highlight the ferroelectric and piezoelectric responses of the PDMS–ZnS:Cu samples, affirming its potential in developing flexible, self-powered devices. The XRD pattern of pure ZnS:Cu particles is shown in Fig. S3. As per the XRD pattern, there is no formation of Zn/Cu metal. The XRD results confirm that the particles exhibit a crystalline wurtzite-type ZnS structure (JCPDF #36-1450), and no noticeable phase deformation. A similar type of XRD pattern for ZnS:Cu was also reported by Gan et al., and they also claim ZnS:Cu has a piezoelectric nature, which can result in the generation of an internal electric field under applied stress.[53] Fig. 1c shows the illustration of the PENG + ML hybrid device, and an optical image is given. The cross-section illustration shows the composite with electrodes, and the encapsulation layer was done with transparent PDMS polymer.

This journal is © The Royal Society of Chemistry 2025
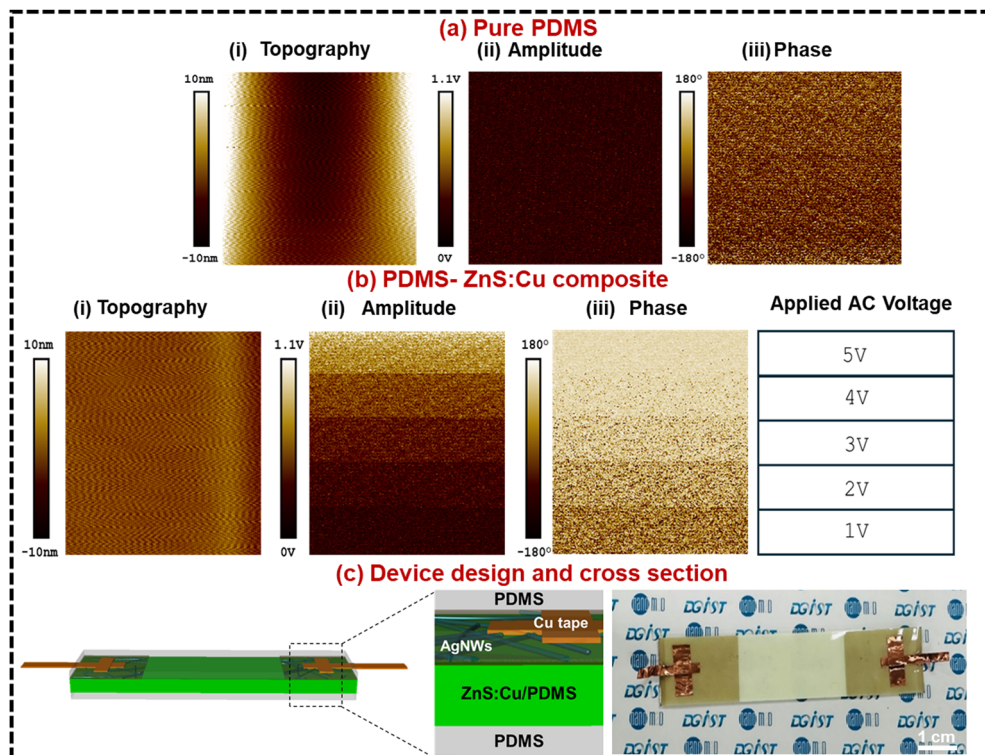
J. Mater. Chem. C, 2025, 13, 19297–19307 | 19299

Fig. 1 (a) Topography and piezoresponse force microscopy images (amplitude and phase) of pure PDMS; (b) topography and piezoresponse force microscopy images (amplitude and phase) of PDMS–ZnS:Cu composites at various applied AC voltage and (c) lllustration of the developed device design along with digital picture of dual-mode PENG-ML device.

The piezoelectric nanogenerator was developed, and the working mechanism in a ZnS:Cu–PDMS composite under stretching relies on the piezoelectric effect in ZnS:Cu particles and the mechanical deformation of the polymer matrix. When mechanical strain is applied, the ZnS:Cu particles experience lattice distortion, inducing a polarization field and generating charge separation across the material. But in the case of the device being subjected to the pressing force, the dipoles are oriented, leading to a piezoelectric polarization. This leads to the generation of electrical output at both ends of the electrodes of PENG. However, the ML generation in the case of the PDMS–ZnS:Cu is randomly emitted by a single particle landscape, which comes from the triboelectric effect, which is a basic phenomenon for the generation of ML. During stretching and bending forces, electroluminescence is generated by triboelectrification at the interface of the pore gap between the positively charged ZnS:Cu particles and negatively charged PDMS polymer.[54]

Fig. 2 shows the detailed synthesis of device fabrication steps using the PDMS–ZnS:Cu composites. Embedded AgNWs were used as electrodes due to their excellent flexibility and high conductivity, allowing seamless integration into stretchable composites. AgNWs are perfect for wearable and dynamic ML sensing applications because, in contrast to rigid electrodes, they retain electrical performance under deformation.[55,56] The top row showcases the initial steps: deposition of conductive Ag nanowires on glass and obtaining the glass coated with

Ag nanowires, further using the tape pattern of the Ag nanowires on glass. The middle-row steps show the mixture of PDMS–ZnS:Cu is spin-coated on the Ag nanowires-coated glass. After the curing process in the oven, the flexible composite is detached. Further, the copper wires were connected to the device. In the end, the encapsulation of the device was done using PDMS to protect the ML + PENG platform from any damage. The device platforms were cut into respective dimensions of 2 cm × 9 cm. Further, the dual-mode PENG-ML device platform was utilized to harvest energy and for various applications in underwater communication.

Fig. 3 shows the electrical output of the device platform under the pushing force. Notably, under pushing force, the electrical output is more dominant than the mechanoluminescent signals. Fig. 3a and b show the electrical voltage and current output of the device platform at a fixed force of 5N. The voltage of 17 V and current of 70 nA were delivered by the device when force was applied to it using a linear motor. Fig. 3c presents the switching polarity test of the developed device. To ensure that the generated voltage comes from the piezoelectric action and not from outside noise or artifacts, it is essential to switch the polarity of a PENG. The dependability of device platform readings can be confirmed if the signal reverses upon polarity change, confirming the true piezoelectric response. Fig. S4 shows the piezoelectric output voltage at various thicknesses of PDMS–ZnS:Cu composite. In a composite-based PENG, increasing the composite film thickness influences electrical output.[57] As thickness increases,
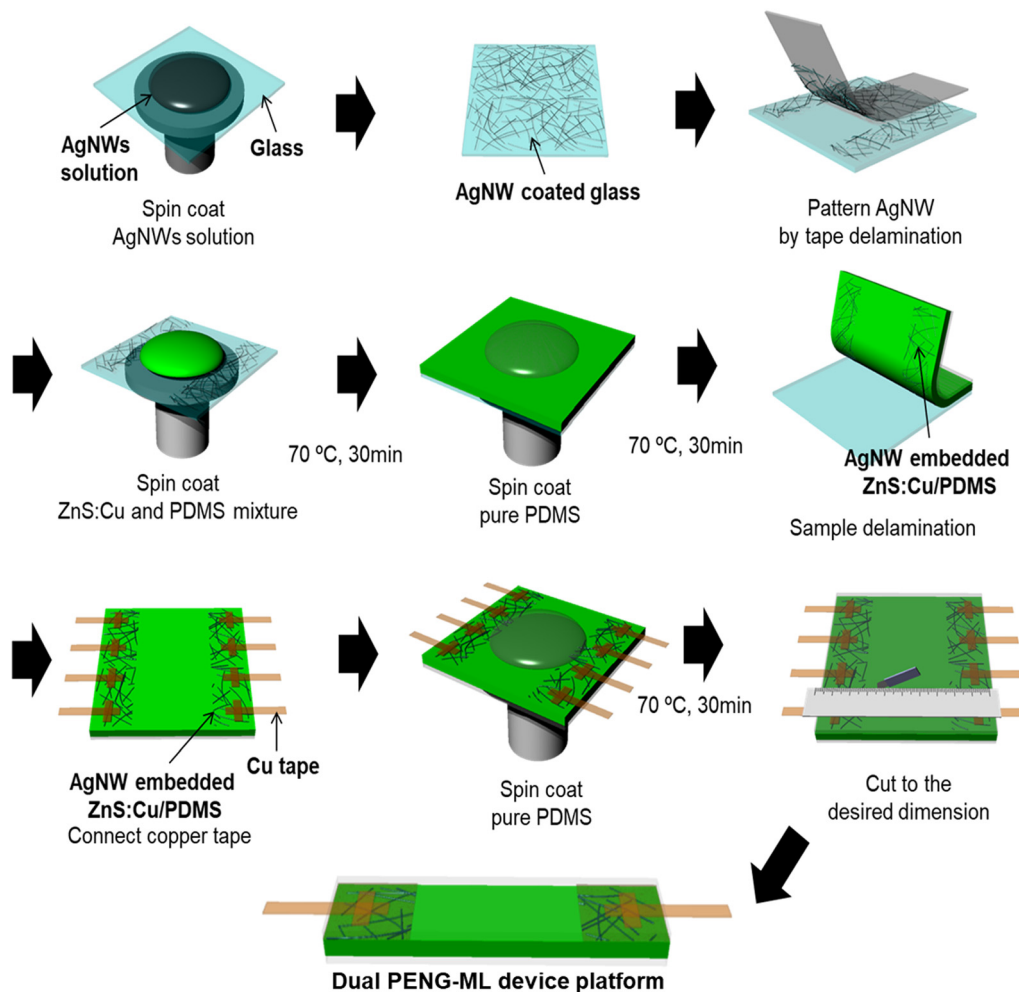
Fig. 2 Step-by-step procedure of the synthesis till design of the dual PENG-ML device platform.

the generated voltage typically rises due to a greater potential difference across the material. Excessive thickness can compromise flexibility and energy conversion efficiency. Fig. S5 shows the comparison of the electrical voltage of PDMS–ZnS:Cu composite-based device with PDMS encapsulation having no air gap and without any PDMS encapsulation having an air gap. The device with no air gap, deformation only strains the piezoelectric layer, generating piezoelectric output. When an air gap is introduced, additional triboelectric charge transfer occurs alongside the piezoelectric effect, increasing the electrical voltage output of the device. Fig. 3d shows the long-term stability of the device under constant force and frequency. The consistent voltage output over 1200 seconds indicates the durability and reliability of the device platform in generating constant performance under repeated mechanical deformation. Fig. 3e shows the voltage generated by the device at various load resistances. This plot illustrates how the output voltage increases with increasing load resistance as per Ohm's law. The power generated by the device is obtained by using the formula $P = V^2/R$ (where V = voltage and R = resistance). Fig. 3f illustrates the curve to shed light upon power output variation as a function of load resistance.

The highest power of 0.36 μW at 250 MΩ is achieved using the pushing force upon the device platform. Fig. 3g plot presents the charging characteristics of different capacitors (0.1–1 μF). Fig. 3h depicts the cyclic charging and discharging of a 0.1 μF capacitor, showing the ability of the PENG to charge the capacitor over multiple cycles. Fig. 3i shows the voltage output when the device is subjected to manual palm pressing. The consistent peak-to-peak output confirms its sensitivity to human-applied forces, indicating its potential use in wearables.

Fig. 4a and b show the voltage and current of the PENG + ML platform by applying a stretching force. The electrical output from the device indicates the generation of piezoelectric output, confirming the ability of the composite to convert mechanical strain into electrical signals. The inset image provides visual evidence of the stretching process. Fig. 4c and d show the voltage, current of the PENG + ML platform by applying a bending force. The voltage and current response recorded under bending deformation demonstrate periodic fluctuations, confirming that the device platform successfully carried out the conversion of mechanical bending forces into electrical signals. The inset shows the bending experiment, emphasizing its adaptability to different mechanical deformations. A stronger
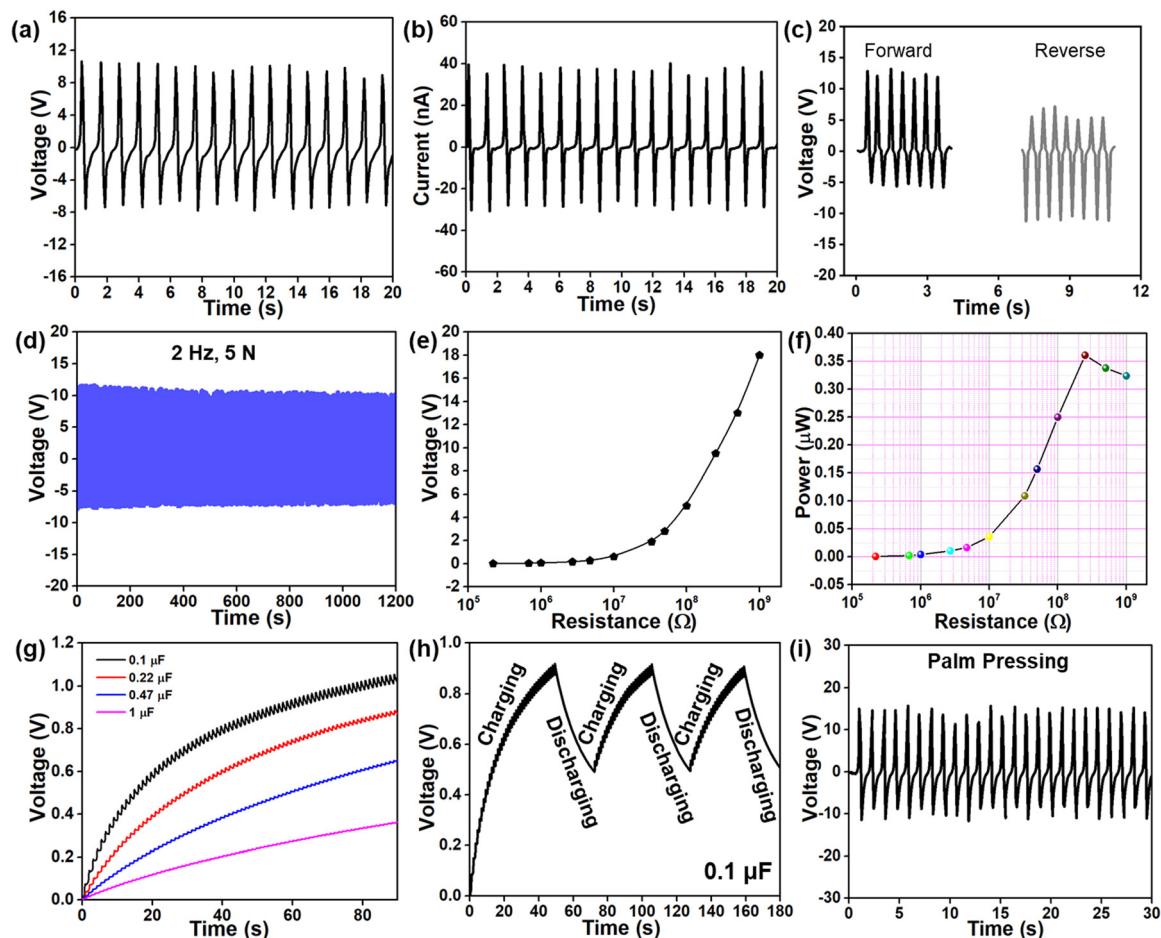
This journal is © The Royal Society of Chemistry 2025

J. Mater. Chem. C, 2025, 13, 19297–19307 | 19301

Fig. 3 (a) Voltage, (b) current of the PENG device based on PDMS: ZnS–Cu, (c) switching polarity test of PENG, (d) Stability test of PENG, (e) and (f) voltage and power of PENG at various load resistances, (g) charging of various capacitors using PENG, (h) charging–discharging curves of 0.1 μF capacitor using PENG and (i) voltage generated by PENG by applying palm pressing.

piezoelectric output is produced by bending because it creates an uneven stress distribution and strain gradient across the material, which improves dipole alignment. Stretching, on the other hand, produces less voltage generation and smaller polarization changes since it provides a more uniform strain. Fig. 4e illustrates the force-dependent voltage response of the PDMS–ZnS:Cu based PENG. As the applied force increases from 2 N to 7 N, the voltage amplitude rises, confirming a direct relationship between mechanical stress and charge generation. This behavior follows the piezoelectric equation ($Q = d_{33} \times F$), where higher force induces greater charge displacement, leading to increased voltage output ($V = Q/C$). This trend demonstrates the sensitivity of the device platform to various mechanical deformations.

Fig. 4 f and g show the digital image of the device platform when the light is ON and OFF. The PDMS–ZnS:Cu composites improved mechanical stress distribution, leading to the ML during bending and stretching. Bending increases ML output by causing compressive stress on one side and tensile stress on the other, which increases charge separation and recombination. Stretching enhances light emission by distorting the ZnS:Cu lattice and maximizing tensile strain. Hence, the

PENG + ML device platform can ensure its applicability in energy harvesting and smart sensing technologies.

Simultaneous PENG energy harvesting and ML emission from a single PENG + ML device platform are showcased in Fig. 5. Fig. 5a–d show the current of the PENG + ML device platform at various stretching %. As strain increases, more dipoles align, leading to greater charge accumulation and raising the voltage output. Fig. 5e–h show the voltage of the PENG + ML device platform at various stretching %. A higher strain% leads to higher charge generation. As stretching increases, the separation between dipoles widens, causing a higher rate of charge displacement, which leads to an increase in current. Fig. 5i–l show the optical images of ML emission from the PENG + ML device platform at various stretching rates. Higher stretching percentages enhance charge separation and recombination at defect locations by increasing lattice distortion in ZnS:Cu particles, which in turn raises ML intensity. Combining triboelectric and piezoelectric effects leads to higher luminescence emission, which is made possible by increased strain. Stronger luminescence emission results from increased stress-induced charge generation, which raises ML efficiency.

19302 | J. Mater. Chem. C, 2025, 13, 19297–19307
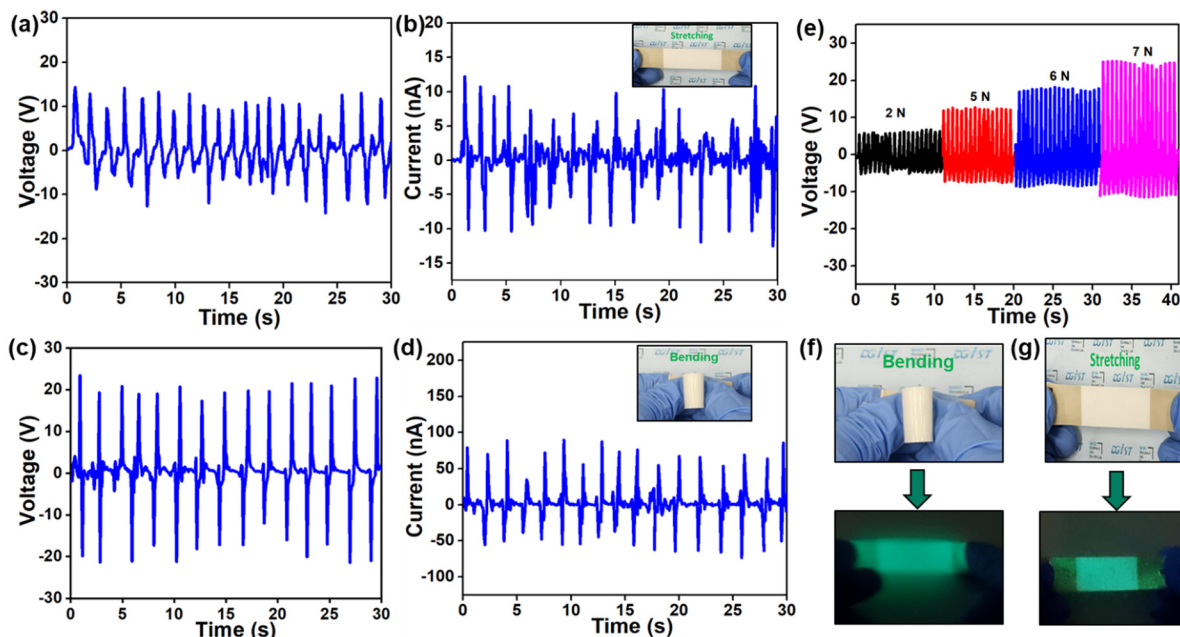
This journal is © The Royal Society of Chemistry 2025

Fig. 4 (a) Voltage of PENG during hand stretching motion, (b) current of PENG during hand stretching motion, (c) voltage of PENG during hand bending motion, (d) current of PENG during hand bending motion, (e) voltage of PENG during various applied forces, (f) and (g) optical images of the ML generated by the PENG device during hand bending and stretching in dark conditions.
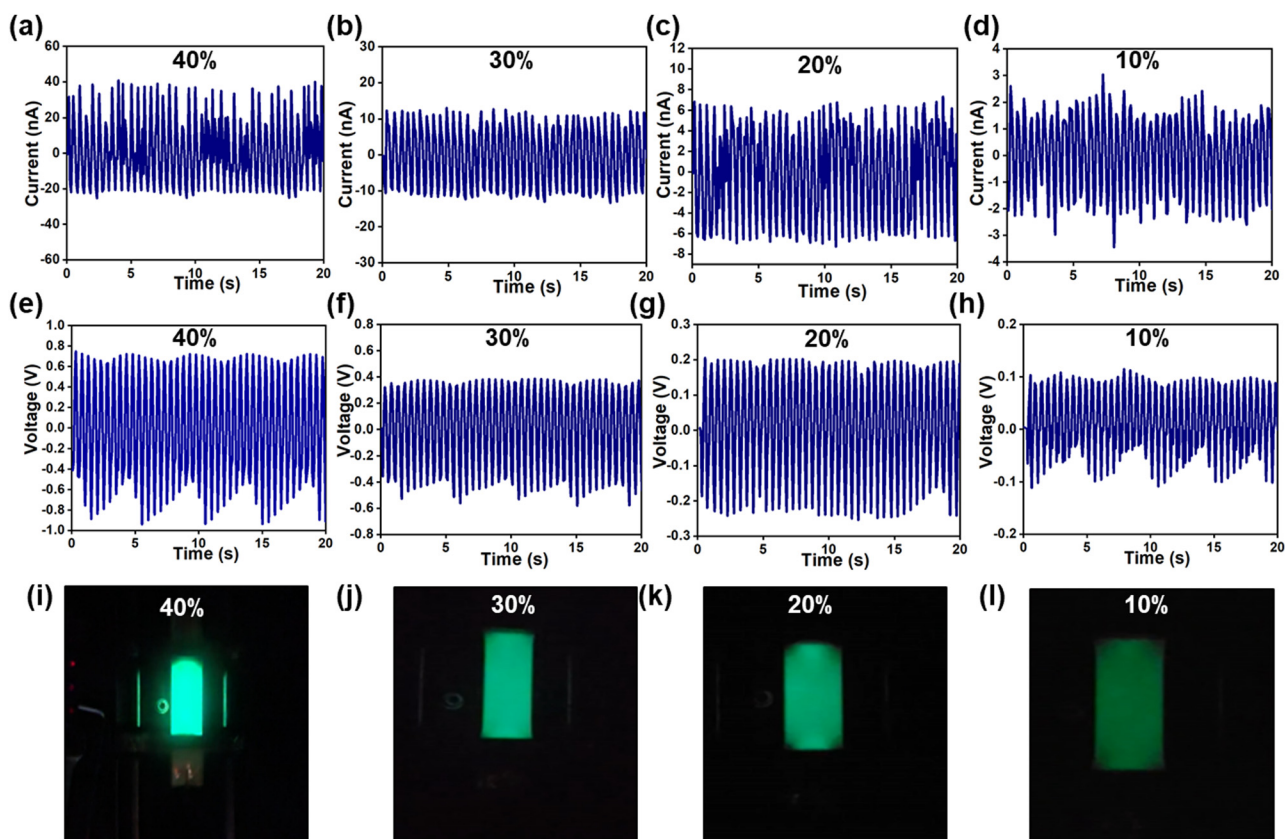

Fig. 5 Simultaneous energy harvesting and ML signals. (a)–(d) Current generated by the PENG device during various elongations 10%, 20%, 30%, and 40% using a stretching machine, (e)–(h) voltage generated by the PENG device during various elongations 10%, 20%, 30%, and 40% using a stretching machine, (i)–(l) digital images of the corresponding ML signal generated during various elongation 10%, 20%, 30% and 40% using a stretching machine.

This journal is © The Royal Society of Chemistry 2025

J. Mater. Chem. C, 2025, 13, 19297–19307 | 19303

The simultaneous PENG + ML at a single device platform was investigated to harvest energy and optical emission. The optical image of the device bending and ML emission of the device platform in Fig. 6a. The voltage and current response of the device platform using bending motions are shown in Fig. 6b and c. The bending motions could generate the ML and piezoelectric energy simultaneously, leading to the effectiveness of this composite to be utilized in self-powered applications. Due to stress-induced charge carrier excitation, which subsequently recombines to produce light, bending motion aids in the generation of ML signals. An internal electric field is produced by mechanical stress that accelerates piezoelectric polarization in the device platform, resulting in an electrical output.

The illustration of the composites being attached to the testing setup for stretching is in Fig. 6d. The microstructure of the cross-section of the device platform in the middle region is shown in Fig. 6e. The encapsulation of the PDMS is done properly without any air gap, confirming that the output of the PENG is not affected by any artifacts or static charges. The stability of the piezoelectric output generated from the device platform of PENG + ML for 300 seconds is shown in Fig. 6f. The 3D visualization of the PDMS–ZnS:Cu composite is seen in

Fig. 6g, which confirms the uniform distribution of ZnS:Cu in the polymer PDMS. Fig. 6h depicts the ML intensity *vs.* wavelength, showing a prominent emission peak at ∼500 nm (green light). The sharp intensity rise indicates efficient stress-induced light emission. The inset confirms the emission of green ML under deformation by the ML + PENG device. Fig. 6i shows the CIE 1931 xy chromaticity diagram maps the emission coordinates within the visible spectrum. The data point falls in the green region, confirming the spectral emission (∼500 nm).

Simultaneous energy harvesting and ML devices are highly beneficial for underwater communication and diver signaling due to their self-powered nature. Without requiring external power sources, these platforms transform mechanical energy into electrical impulses and luminescence. Furthermore, ML emission is less impacted by salinity and water turbulence, guaranteeing communication, navigation, and sea rescue. Fig. 7a shows the driver under the water wearing bands for emitting ML and PENG signals while bending the wrist while signaling various signals such as "dizziness", "I am reserved", and "narcosis". During the bending motion of the wrist at the interface of the ZnS:Cu microparticles and polymer PDMS, triboelectricity is created, leading to the generation of ML. Fig. 7b–d show the simultaneous ML and PENG voltage output
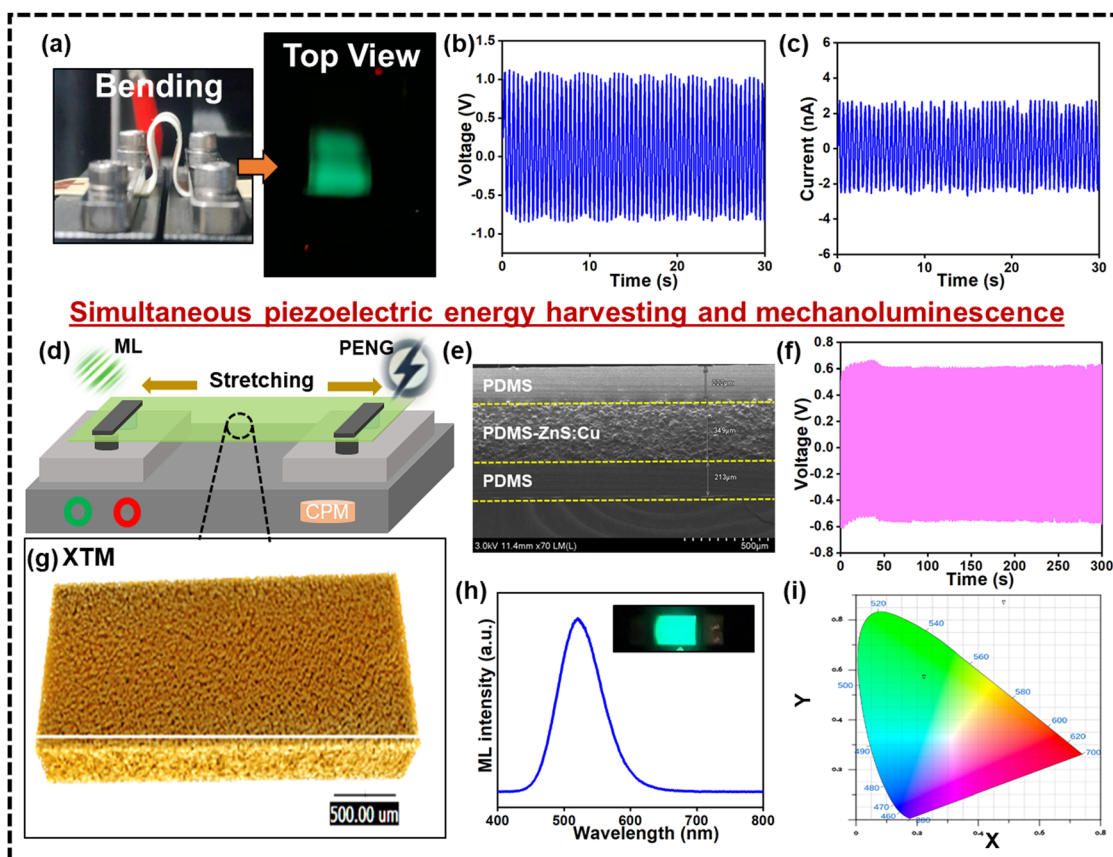

Fig. 6   (a) Digital image of the PENG device in bending state using the stretching machine and corresponding ML, (b)–(c) voltage and current recorded simultaneously while bending of PENG, (d) illustration of the PENG device attached to stretching machine for simultaneous ML and PENG, (e) cross-section morphology of the packed PENG device, (f) voltage stability of the PENG device while stretching, (g) X-ray tomographic image of the PDMS-ZnS:Cu composite, (h) ML intensity when the PENG device was stretched and (i) corresponding CIE coordinates.
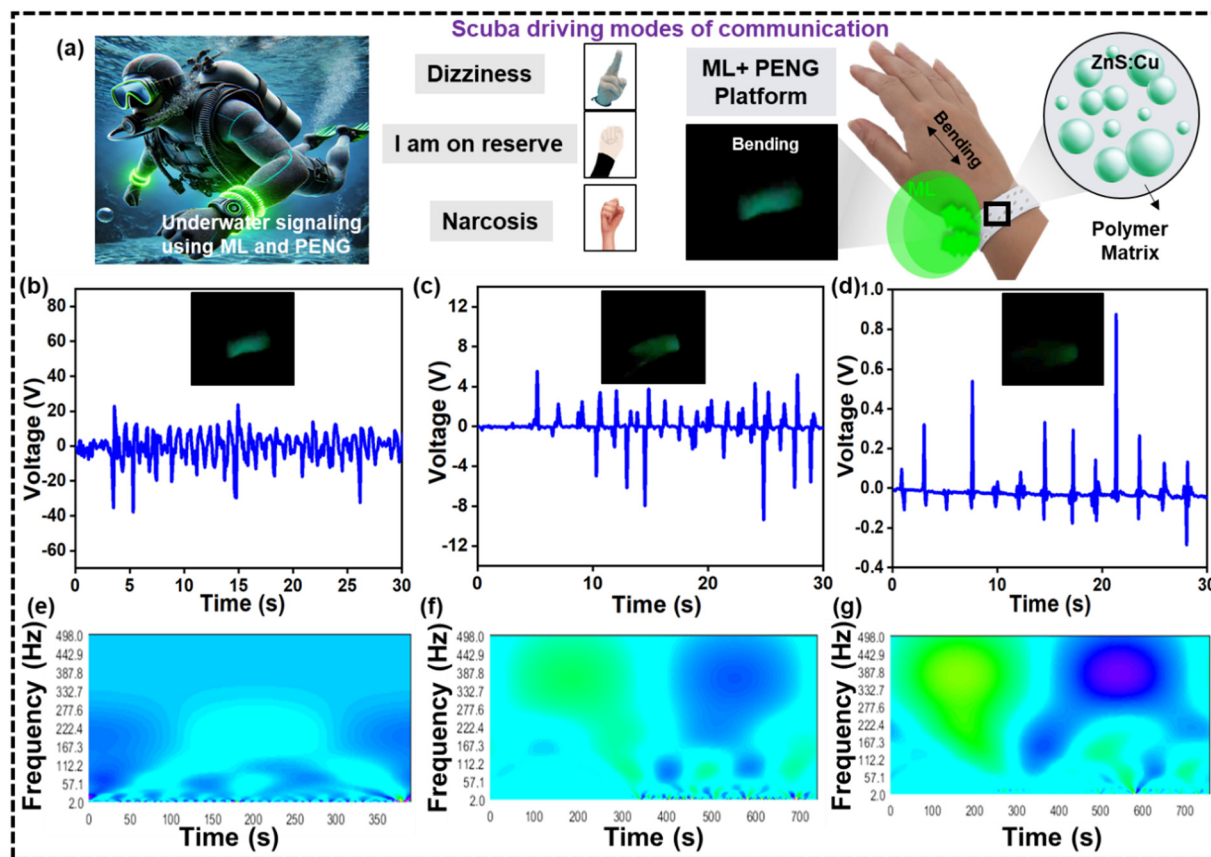
Fig. 7 (a) 3D illustration of the simultaneous ML and Energy harvesting signal under water and corresponding hand signal employed by drivers for communication, (b)–(d) simultaneous ML and voltage signals generated by the PENG attached in the wrist of the driver, and (e)–(g) FFT signals of the corresponding voltage signals generated by PENG device.

generated by the device platform under various signaling underwater. Fast Fourier Transform (FFT) decomposes a complex signal into sin and cos components, revealing dominant frequencies and aiding in signal filtering, feature extraction, and frequency-based analysis. The signals generated by the PENG + ML device can be precisely analyzed by FFT technology, which effectively transforms time-domain data into the frequency domain as shown in Fig. 7e–g. By differentiating various frequency components, it aids in the detection of noise, mechanical responses, and periodic patterns. Device signals and signal processing techniques help in performance optimization, and efficiency enhancement, which paves the way for several applications, including structural health monitoring, energy harvesting, underwater communication, wearable electronics for real-time data analysis.

fabrication of a lead-free piezoelectric elastomer by directly incorporating ZnS:Cu into an elastomer matrix. The composites were constructed using the spin coating technique, a simple and cost-effective approach. The sensor demonstrates long-term stability for generating electrical and optical responses, making it a proper candidate for extended operation under continuous mechanical stress. The device platform has high adaptability to real-world applications as it can respond to stress, bend, and press motions, generating both electrical as well as optical responses. Overall, this hybrid platform of ML and PENG exhibits broad potential in wearable devices, smart interfaces, intelligent surveillance, and sustainable energy solutions, making it a valuable advancement in next-generation sensing technologies.

4. Conclusions

A piezoelectric/ML sensor platform with dual-functional output has been developed, capable of generating both electrical and optical signals in response to mechanical forces. The integration of two phenomena in a single device enables a detailed assessment of mechanical deformations. The fabrication process of the device design has been introduced, streamlining the

Author contributions

Sugato Hajra: conceptualization, writing – original draft, formal analysis; **Swati Panda:** formal analysis; **Kushal Ruthvik Kaja:** data curation; **Seongkyu Song:** data curation; **Yeonkyeong Ryu:** investigation; **Basanta Kumar Panigrahi:** visualization; **Naratip Vittaya-korn:** writing – editing and review; **Ju-Hyuck Lee:** investigation, writing – editing and review; **Soon Moon Jeong:** supervision,

This journal is © The Royal Society of Chemistry 2025

J. Mater. Chem. C, 2025, **13**, 19297–19307 | **19305**

Conflicts of interest

The authors have declared no conflict of interest.

Data availability

The data supporting the findings of this study are available from the corresponding author upon reasonable request. All relevant data generated or analyzed during this study are included in this published article.

Supplementary information is available. See DOI: https://doi.org/10.1039/d5tc02181b

Acknowledgements

References

1 B. Chen, X. Zhang and F. Wang, *Acc. Mater. Res.*, 2021, **2**, 364–373.

2 S. Song, B. Song, C.-H. Cho, S. K. Lim and S. M. Jeong, *Mater. Today*, 2020, **32**, 46–58.

3 J. Luo, B. Ren, X. Zhang, M. Zhu, T. Liang, Z. Huang, Y. Zheng, X. Li, J. Li and Z. Zheng, *Adv. Sci.*, 2024, **11**, 2305066.

4 J. Zhao, S. Song, X. Mu, S. M. Jeong and J. Bae, *Nano Energy*, 2022, **103**, 107825.

5 S. M. Jeong, S. Song and H. Kim, *Nano Energy*, 2016, **21**, 154–161.

6 Z. Huang, B. Chen, B. Ren, D. Tu, Z. Wang, C. Wang, Y. Zheng, X. Li, D. Wang, Z. Ren, S. Qu, Z. Chen, C. Xu, Y. Fu and D. Peng, *Adv. Sci.*, 2023, **10**, 2204925.

7 S. A. Behera, S. Panda, S. Hajra, K. R. Kaja, A. K. Pandey, A. Barranco, S. M. Jeong, V. Vivekananthan, H. J. Kim and P. G. R. Achary, *Adv. Sustainable Syst.*, 2024, **8**, 2400344.

8 K. Parida, J. Xiong, X. Zhou and P. S. Lee, *Nano Energy*, 2019, **59**, 237–257.

9 A. Alagumalai, O. Mahian, K. E. K. Vimal, L. Yang, X. Xiao, S. Saeidi, P. Zhang, T. Saboori, S. Wongwises, Z. L. Wang and J. Chen, *Nano Energy*, 2022, **101**, 107572.

10 D. P. Boden, *J. Power Sources*, 2004, **133**, 47–51.

11 S. Yong, J. Wang, L. Yang, H. Wang, H. Luo, R. Liao and Z. L. Wang, *Adv. Energy Mater.*, 2021, **11**, 2101194.

12 K. R. Kaja, S. Hajra, S. Panda, M. A. Belal, U. Pharino, H. Khanbareh, N. Vittayakorn, V. Vivekananthan, C. Bowen and H. J. Kim, *Nano Energy*, 2024, 110319.

13 S. Panda, S. Hajra, Y. Oh, W. Oh, J. Lee, H. Shin, V. Vivekananthan, Y. Yang, Y. K. Mishra and H. J. Kim, *Small*, 2023, **19**, 2300847.

14 W. Zhang, Y. Gui, Y. Yang and C. Tang, *J. Cleaner Prod.*, 2023, **429**, 139550.

15 A. Babu, K. Ruthvik, P. Supraja, M. Navaneeth, K. U. Kumar, R. R. Kumar, K. Prakash and N. Raju, *J. Mater. Sci.: Mater. Electron.*, 2023, **34**, 2195.

16 Z. L. Wang and J. Song, *Science*, 2006, **312**, 242–246.

17 S. Panda, S. Hajra, H. Jeong, B. K. Panigrahi, P. Pakawanit, D. Dubal, S. Hong and H. J. Kim, *Nano Energy*, 2022, **102**, 107682.

18 V. Vivekananthan, A. Chandrasekhar, N. R. Alluri, Y. Purusothaman, W. Joong Kim, C.-N. Kang and S.-J. Kim, *Mater. Lett.*, 2019, **249**, 73–76.

19 A. N. Filippin, J. R. Sanchez-Valencia, X. Garcia-Casas, V. Lopez-Flores, M. Macias-Montero, F. Frutos, A. Barranco and A. Borras, *Nano Energy*, 2019, **58**, 476–483.

20 C. Zhang, Z. Jiang, M. Sun, R. Augustin-Lawson, S. H. Kwon and L. Dong, *Nano Energy*, 2025, **136**, 110755.

21 S. Hajra, S. Sahoo and R. N. P. Choudhary, *J. Polym. Res.*, 2018, **26**, 14.

22 S. Panda, S. Hajra, K. Mistewicz, P. In-na, M. Sahu, P. M. Rajaitha and H. J. Kim, *Nano Energy*, 2022, **100**, 107514.

23 S. Hajra, Y. Oh, M. Sahu, K. Lee, H.-G. Kim, B. K. Panigrahi, K. Mistewicz and H. J. Kim, *Sustainable Energy Fuels*, 2021, **5**, 6049–6058.

24 T. Li and P. S. Lee, *Small Struct.*, 2022, **3**, 2100128.

25 K. Mistewicz, M. Jesionek, H. J. Kim, S. Hajra, M. Kozioł, L. Chrobok and X. Wang, *Ultrason. Sonochem.*, 2021, **78**, 105718.

26 S. Hajra, S. Panda, S. Song, B. K. Panigrahi, P. Pakawanit, S. M. Jeong and H. J. Kim, *Nano Energy*, 2023, **114**, 108668.

27 K.-S. Sohn, S. Timilsina, S. P. Singh, J.-W. Lee and J. S. Kim, *ACS Appl. Mater. Interfaces*, 2016, **8**, 34777–34783.

28 X. Wang, M. Que, M. Chen, X. Han, X. Li, C. Pan and Z. L. Wang, *Adv. Mater.*, 2017, **29**, 1605817.

29 X. Zhang, Z. Li, W. Du, Y. Zhao, W. Wang, L. Pang, L. Chen, A. Yu and J. Zhai, *Nano Energy*, 2022, **96**, 107115.

30 M. He, W. Du, Y. Feng, S. Li, W. Wang, X. Zhang, A. Yu, L. Wan and J. Zhai, *Nano Energy*, 2021, **86**, 106058.

31 S. Hajra, S. Panda, S. Song, H. Song, B. K. Panigrahi, S. M. Jeong, Y. K. Mishra and H. J. Kim, *Adv. Sustainable Syst.*, 2024, **8**, 2400609.

32 C. N. Xu, T. Watanabe, M. Akiyama and X. G. Zheng, *Appl. Phys. Lett.*, 1999, **74**, 2414–2416.

33 Z. Huang, X. Li, T. Liang, B. Ren, X. Zhang, Y. Zheng, Q. A. Zhang, Z. Fang, M. Wu, M. Zulfiqar, L. Jing, S. Qu, B. Chen, J. Gan and D. Peng, *Responsive Mater.*, 2024, **2**, e20240019.

34 S. M. Jeong, S. Song, S.-K. Lee and N. Y. Ha, *Adv. Mater.*, 2013, **25**, 6194–6200.

35 S. Moon Jeong, S. Song, S.-K. Lee and B. Choi, *Appl. Phys. Lett.*, 2013, **102**, 051110.

36 F. Yang, Y. Yuan, R. P. Sijbesma and Y. Chen, *Macromolecules*, 2020, **53**, 905–912.

37 A. F. Banishev and A. A. Banishev, *Inorg. Mater.: Appl. Res.*, 2019, **10**, 647–651.

38 X. Qian, Z. Cai, M. Su, F. Li, W. Fang, Y. Li, X. Zhou, Q. Li, X. Feng, W. Li, X. Hu, X. Wang, C. Pan and Y. Song, *Adv. Mater.*, 2018, **30**, 1800291.

19306 | *J. Mater. Chem. C*, 2025, **13**, 19297–19307

This journal is © The Royal Society of Chemistry 2025

39 W. Wang, Z. Wang, J. Zhang, J. Zhou, W. Dong and Y. Wang, *Nano Energy*, 2022, **94**, 106920.

40 H. I. Jeong, H. S. Jung, M. Dubajic, G. Kim, W. H. Jeong, H. Song, Y. Lee, S. Biswas, H. Kim, B. R. Lee, J. W. Yoon, S. D. Stranks, S. M. Jeong, J. Lee and H. Choi, *Nat. Commun.*, 2025, **16**, 854.

41 C. Wang, R. Ma, D. Peng, X. Liu, J. Li, B. Jin, A. Shan, Y. Fu, L. Dong, W. Gao, Z. L. Wang and C. Pan, *InfoMat*, 2021, **3**, 1272–1284.

42 X. Sun, S. Ling, Z. Qin, J. Zhou, Q. Shi, Z. Liu and Y. J. Tan, *Adv. Mater.*, 2025, 2502743.

43 B. Lu, Y. Chen, D. Ou, H. Chen, L. Diao, W. Zhang, J. Zheng, W. Ma, L. Sun and X. Feng, *Sci. Rep.*, 2015, **5**, 16065.

44 P. Sharma, S. Hajra, S. Sahoo, P. K. Rout and R. N. P. Choudhary, *Process. Appl. Ceram.*, 2017, **11**, 171–176.

45 S. A. Behera, S. Panda, S. Hajra, B. K. Panigrahi, H. J. Kim and P. G. R. Achary, *Energy Technol.*, 2023, **11**, 2300469.

46 S. Tunstall and D. Amarasiriwardena, *Microchem. J.*, 2002, **73**, 335–347.

47 S. Korkmaz and I. A. Kariper, *J. Electroceram.*, 2022, **48**, 8–34.

48 Y. He, Z. Wang, X. Hu, Y. Cai, L. Li, Y. Gao, X. Zhang, Z. Huang, Y. Hu and H. Gu, *RSC Adv.*, 2017, **7**, 16908–16915.

49 S. Wang, H. Liu, Y. Wang, H. Qin, J. Zhao, Z. Lu, Z. Mao and D. Wang, *J. Am. Ceram. Soc.*, 2024, **107**, 205–213.

50 D. K. Khatua and S.-J. Kim, *J. Mater. Chem. C*, 2022, **10**, 2905–2924.

51 S. Maity, A. Sasmal and S. Sen, *Mater. Sci. Semicond. Process.*, 2023, **153**, 107128.

52 J. Anthoniappen, W. S. Chang, A. K. Soh, C.-S. Tu, P. Vashan and F. S. Lim, *Acta Mater.*, 2017, **132**, 174–181.

53 J. Gan, M. G. Kang, M. A. Meeker, G. A. Khodaparast, R. J. Bodnar, J. E. Mahaney, D. Maurya and S. Priya, *J. Mater. Chem. C*, 2017, **5**, 5387–5394.

54 G. Lee, S. Song, W. H. Jeong, C. Lee, J.-S. Kim, J.-H. Lee, J. Choi, H. Choi, Y. Kim, S. J. Lim and S. M. Jeong, *Small*, 2024, **20**, 2307089.

55 R. Karimi-Chaleshtori, A. H. Nassajpour-Esfahani, M. R. Saeri, P. Rezai and A. Doostmohammadi, *Mater. Today Chem.*, 2021, **21**, 100496.

56 F. Xu and Y. Zhu, *Adv. Mater.*, 2012, **24**, 5117–5122.

57 O. Y. Pawar and S. Lim, *J. Appl. Polym. Sci.*, 2024, **141**, e56234.

This journal is © The Royal Society of Chemistry 2025

J. Mater. Chem. C, 2025, **13**, 19297–19307 | **19307**